Histol Histopathol (2014) 29: 1185-1199
DOI: 10.14670/HH-29.1185

http://www.hh.um.es

Histology and Histopathology
Cellular and Molecular Biology

Aberrant expressions of delta-protocadherins in the brain of Npc1 mutant mice

Xin Yan[1], Jan Lukas[1], Juntang Lin[2], Mathias Ernst[3], Dirk Koczan[4], Martin Witt[5], Georg Fuellen[3], Andreas Wree[5], Arndt Rolfs[1] and Jiankai Luo[1]

[1]Albrecht-Kossel-Institute for Neuroregeneration, Rostock University Medical Center, Rostock, Germany, [2]Institute of Anatomy I, School of Medicine University of Jena, Jena, Germany, [3]Institute for Biostatistics and Informatics in Medicine and Ageing Research, University of Rostock,Rostock, Germany, [4]Institute for Immunology, Rostock University Medical Center, Rostock, Germany and [5]Institute of Anatomy, Rostock University Medical Center, Rostock, Germany

Summary. Niemann-Pick type C1 (NPC1) disease is an autosomal recessive disorder characterized by dysmyelination and neurodegeneration, which can result in the death of patients in early childhood in some cases. Members of the delta-protocadherins (Pcdhs) play important roles in neurogenesis and brain development. In this study, we compared expression profiles of Pcdhs in the brain between wild-type and Npc1 mutant mice from postnatal day (P) 9 onwards by in situ hybridization. Our data show that laminar distribution of some Pcdhs in the cerebral cortex of Npc1 mutated mice is different from that of wild-type mice. Furthermore, expressions of Pcdhs by oligodendrocytes in the corpus callosum and by Purkinje cells and granular cells in the cerebellum are strongly decreased in Npc1 mutated mice at later stages. Taken together, our data suggest that aberrant expression of Pcdhs is a pathological process accompanied by neurodegeneration in Npc1 mutant mice.

Key words: NPC1, Delta-protocadherins, Gene expression, Mouse

Introduction

Niemann-Pick type C (NPC) disease is an autosomal recessive disorder characterized by cellular accumulation of unesterified cholesterol and glycosphingolipids. Approximately, 95% of NPC disease is caused by mutations of Npc1 gene and 5% of Npc2 gene (Carstea et al., 1997; Loftus et al., 1997; Naureckiene et al., 2000). Both Npc proteins collaborate in processes of transporting intracellular cholesterol from lysosomes to the endoplasmic reticulum and Golgi apparatus (Carstea et al., 1997; Vanier and Millat, 2003). Different mutations of Npc1 gene typically cause dysmyelination and axonal swelling, resulting in neuronal death in early childhood, and subsequently leading to motor impairment in the central nervous system (CNS) of the patients (Pentchev et al., 1984; Bauer et al., 2002; Võikar et al., 2002; Baudry et al. 2003).

The Npc1 mutant ($Npc1^{-/-}$) mouse is usually asymptomatic at birth, but gradually develops neurological symptoms, including tremor and ataxia from about seven weeks onwards (Ong et al., 2001; Luan et al., 2008). $Npc1^{-/-}$ mice show spatio-temporally pathological changes, e.g., loss of neurons in the prefrontal cortex, thalamus and brainstem, predominant loss of Purkinje cells in the cerebellum; myelination defects in the cerebral cortex, the hippocampus and in the middle layer of the corpus callosum; and activation of microglia and astrocytes (German et al., 2002; Baudry et al., 2003; Sarna et al., 2003). Furthermore, experiments have demonstrated cognitive impairment for learning and remembering in $Npc1^{-/-}$ mice (Võikar et al., 2002; Hovakimyan et al., 2013). All these pathologies mimic a phenotype similar to human NPC1 patients.

Cadherins are Ca^{2+}-dependent cell adhesion molecules involved in neurogenesis and functional neural networks (Hirano et al., 2003; Luo et al., 2004; Redies et al., 2003, 2005; Takeichi, 2007; Hulpiau and

Offprints requests: Dr. Jiankai Luo, Albrecht-Kossel-Institute for Neuroregeneration, Rostock University Medical Center, Gehlsheimer Strasse 20, 18147 Rostock, Germany. e-mail: jiankai.luo@uni-rostock.de

van Roy, 2009). Protocadherins, members of the cadherin family, play important roles in multiple processes, including gray matter differentiation, axon pathfinding, target recognition, and synaptogenesis (Homayouni et al., 2001; Uemura et al., 2007; Emond et al., 2009; Liu et al., 2010).

Members of delta-protocadherins (Pcdhs) of the protocadherin subfamily are expressed under specific spatial and temporal conditions in the developing and mature vertebrate brain, contributing to generation of complex neural networks and regulation of brain function (Aoki et al., 2003; Hirano, 2007; Liu et al., 2009, 2010; Hertel and Redies, 2011). Abnormality of Pcdhs is associated with neurological disorders and diseases (Ostergaard et al., 2010; Miyake et al., 2011; Miar et al., 2011; Redies et al., 2011, 2012; Kahr et al., 2013). For example, Pcdh9 expression is downregulated in cerebral glial tumors (Wang et al., 2012), while PcdhB1 and Pcdh7 are up-regulated in postmortem brains of Rett syndrome patients. A mutation of Pcdh15, a key molecule forming the link between neighboring hair cells in the cochlea, is associated with both syndromic and non-syndromic hearing loss (Alagramam et al., 2001; Ahmed et al., 2003; Sliwinska-Kowalska and Pawelczyk, 2013). Pcdh19 is predicted to be involved in the establishment of neuronal connections and in synaptic transduction (Yagi and Takeichi, 2000) and a defect of Pcdh19 results in epilepsy and mental retardation (Jamal et al., 2010). Furthermore, Pcdh10 promotes growth of striatal axons and thalamocortical projections (Uemura et al., 2007) and defective Pcdh10 causes an autism-spectrum disorder (Tsai et al., 2012).

The main pathologies of the NPC1 disease are the loss of neurons in the cerebral cortex and of Purkinje cells in the cerebellar cortex. Pcdhs are expressed in the cortical layers (Krishna-K et al., 2011) and their combinatorial expression patterns in the cortical layers are disrupted under a pathological condition (Hertel and Redies, 2011). Therefore, it is of interest to know whether the spatio-temporal expression of Pcdhs is altered in $Npc1^{-/-}$ mice. In the present study, our data show that perturbation of Pcdhs expression accompanies the phenotypes of the $Npc1^{-/-}$ mouse.

Materials and methods

Animals and tissue preparation

Inbred pairs of heterozygous Npc1-mutated mice (BALB/cNctr-$Npc1^{m1N}$/J), purchased from Jackson Laboratory (Bar Harbor, ME, USA), were used to generate control wild ($Npc1^{+/+}$) and $Npc1^{-/-}$ mice. After being deeply anesthetized with pentobarbital, for Western blots, mice were killed by decapitation and the cerebral cortex was rapidly separated and collected; for immunohistochemistry and electron microscopy, mice were killed by cardiac perfusion with phosphate-buffered saline (PBS), followed by 4% para-formaldehyde in 0.1 M PBS. Then brains were removed and postfixed overnight in the same fixation solution. At least 3 samples for each genotype at postnatal day (P) 9, P30, P49 and P62 were used for this study. Animal experiments were conducted in compliance with the rules and regulations of the local ethical committee and the NIH Guide for the Care and Use of Laboratory Animals.

For RNA profiling analysis by microarrays, fresh tissues of the forebrain, the hindbrain and the cerebellum were separated. Tissue perseveration was done using RNAlater (Ambion, lifetechnologies) according to the manufacturer's recommendation and stored in a freezer (-80°C). At least 6 samples for each genotype at P35 were used for this study.

In situ hybridization

Digoxigenin-labeled cRNA probes were synthesized in vitro using plasmids containing the sequences of different Pcdhs as described previously (Hertel and Redies, 2011) and in situ hybridization on cryosections was performed according to the previous protocol (Lin et al., 2013). Briefly, cryostat sections were pre-treated with proteinase K and acetic anhydride, and hybridization was performed with a cRNA probe in a concentration of 1-2 ng/μl overnight at 70°C in hybridization solution. Subsequently, alkaline phosphatase-coupled anti-digoxigenin Fab fragments (Roche) were used to couple the cRNA probe at 4°C overnight, followed by a enzymatic reaction by adding a mixed substrate solution of nitroblue tetrazolium salt (NBT) and 5-bromo-4-chloro-3-indoyl phosphate (BCIP). The resulting signal in the sections was detected and documented using a microscope system BZ-8000 (Keyence Deutschland GmbH, Neusenburg, Germany). Photographs were adjusted in contrast and brightness by the Photoshop software (Adobe, Mountain View, CA).

For all quantification analyses, Image J software was used to quantify the intensity of Pcdhs in the cortical regions from original bright-field images. The average intensity of the detected regions was measured from 3 images per slide for comparison between $Npc1^{-/-}$ and control brains. At least 3 samples for each genotype of mice at postnatal day (P) 9, P30 and P49 were analyzed for this study.

Antibodies and immunohistochemistry

Primary mouse, rabbit or rat antibodies raised against astrocyte (GFAP; DAKO, Hamburg, Germany), oligodendrocyte (MBP; Convance, California, USA), neuron (NeuN; Chemicon, Darmstadt, Germany), and neurofilament (NF; Abcam) were used. Appropriate Alexa 488- (Molecular Probes, Eugene, USA) or Cy3-labeled (Dianova, Hamburg, Germany) antibodies against mouse, rabbit or rat IgG served as secondary antibodies.

Double fluorescent immunostaining was performed on cryosections according to the method described

previously (Yan et al., 2011). Briefly, after postfixation with 4% formaldehyde, cryosections were blocked with a milk solution (5% skimmed milk and 0.3% Triton X-100 in TBS) at room temperature for 60 min. Then sections were incubated overnight at 4°C with the primary antibody NF, followed by the Alexa-488-labeled secondary antibody (Molecular Probes). After a further blocking step, the sections were incubated with the primary antibody MBP at 4°C overnight. Subsequently, the Cy3-labeled secondary antibody (Dianova) was applied. Finally, cell nuclei were counterstained with 4',6-diamidino-2-phenylindole (DAPI; Sigma). Fluorescence was imaged under a fluorescent microscopy system (BZ-8000; Keyence Deutschland GmbH, Germany). Digital images were adjusted in contrast and brightness with the Photoshop software (Adobe Systems).

Double staining for in situ hybridization and immunostaining was performed in the same section according to the method described previously (Lin et al., 2010).

Western blot analysis

Semiquantitative western blot detection was carried out using the Odyssey Infrared Imaging System (LI-COR Biosciences GmbH, Bad Homburg, Germany) according to protocol described previously (Yan et al., 2011). The primary antibodies of anti-Pcdh10 (1:1000, EMELCA Bioscience) and anti-Pcdh17 (1:1000, EMELCA Bioscience) were used. The antibody of anti-GAPDH (1:10000, Abcam) was used as a loading control. Alexa-Fluor 680 and goat anti-mouse IRDye 800 (1:10.000; Invitrogen) were used as secondary antibodies.

RNA array analysis

Samples stored in RNAlater were lysed in a chaotropic buffer (RNeasy, Qiagen, Hilden) using a FastPrep-24 device (MP Biomedicals) and disposable Lysings Matrix D tubes (BIO 101 Systems). After an additional phenol extraction, the RNAeasy spin column (Qiagen) chromatography protocol was adapted according to the manufacture's guidance. Quality control of the obtained RNA was carried out by a lab on a chip electrophoresis (Bioanalyzer, Agilent) and spectro-photometrical quantification followed by a Nanodrop device (Thermo Fisher).

To perform the Profiling study, Affymetrix GeneChip Mouse Gene 1.0 ST Arrays were hybridized following the Affymetrix WT (whole transcriptome) protocol. Briefly, RNA samples of 200 ng were reverse transcribed introducing a T7 promoter sequence randomly ending with N_6 to all RNA molecules (Ambion WT Expression Kit, Ambion lifetechnologies). Then *in vitro* transcription reaction was performed via the linear amplification protocol using T7 polymerase. After magnet bead based cleanup and spectro-photometrical quantification, twelve microgram cRNA per sample were used to generate a random primed strand-identical new cDNA (GeneChip WT Terminal Labeling and Hybridization Kit, Affymetrix). End labeling was performed using terminal deoxynucleotidyl transferase.

Hybridisation was carried out over night at 45°C in the GeneChip® Hybridisation Oven 640 (Affymetrix) and the microarray was scanned using the GeneChip Scanner 3000 (Affymetrix) at 0.7 micron resolution. All microarray analyses were performed with the statistical programming software R/Bioconductor and the array quality was assessed using the R/Bioconductor package affyPLM (Bolstad et al., 2004, 2005, Brettschneider et al., 2008). Based on the quality control, all arrays were of sufficient quality except one hindbrain sample, which was deleted from the analysis due to quality concerns. Array pre-processing was performed separately for each tissue and consisted of background correction by RMA (Irizarry et al., 2003), and quantile normalization and summarization by median polish. Differential expression of genes was determined by two-sided, unpaired t-tests.

Statistical analysis

Results were reported as mean ± SEM from at least three independent experiments. Statistical evaluation was carried out using the two-tailed Student's t-test with Excel software (Microsoft, USA). A difference was considered to be significant, when the p-value was less than 0.05 (* $p<0.05$; ** $p<0.01$; *** $p<0.001$).

Results

Previous studies have demonstrated that members of the Pcdh family are expressed in the embryonic and adult brain (Redies et al., 2008; Krishna-K et al., 2011) and mutation of reelin protein in the reeler mouse results in an aberrant laminar distribution of the Pcdhs in the cerebral cortex (Hertel and Redies, 2011). In this study, we compared expression patterns of Pcdhs in wild-type and $Npc1^{-/-}$ mice at P9, P30, and P49 in different regions of the brain using antisense cRNA probes, and sense cRNA probes were used as negative controls (e.g., Fig. 2D). The regions of the retrosplenial granular cortex (RSG), the retrosplenial dysgranular cortex (RSD) and the visual cortex (V2) were confirmed visually by comparing structures of the investigated sections with the mouse brain atlas (Franklin Keith and Paxinos, 2007). Results were ordered and presented by regions and developmental stages (from early to late). Fig. 1, Fig. 2 and Fig. 3 show expression patterns of Pcdhs in RSG, RSD and/or V2; Fig. 4 shows quantitative analyses of Pcdhs in the different regions of the cortex; Fig. 5 and Fig. 6 show expression patterns of Pcdhs in the corpus callosum; Fig. 7 in the hippocampus; Fig. 8 in the cerebellum; and Fig. 9 demonstrates the microarray analysis of Pcdh mRNAs in the forebrain. Generally, our results showed that the expression of Pcdhs in the

anatomical structures of the CNS investigated here was altered in Npc1$^{-/-}$ mice compared to wild-type mice.

Pcdhs expression in the cortex at P9

In the cortex region (Fig. 1A), thionin staining revealed that cell distribution and layer structures were similar in both wild-type and Npc1$^{-/-}$ mice (Fig. 1B,C). Expression patterns of Pcdhs, including protocadherin-1 (Pcdh1), Pcdh7, Pcdh9, Pcdh10, Pcdh17, and Pcdh19 between wild-type and Npc1$^{-/-}$ mice were similar (Fig. 1D-O), but in Npc1$^{-/-}$ mice signals of Pcdh7 (Fig. 1G), Pcdh9 (Fig. 1I), Pcdh10 (Fig. 1K), Pcdh17 (Fig. 1M), and Pcdh19 (Fig. 1O) were stronger compared to wild type mice (Fig. 1D,F,H,J,L,N).

Furthermore, we also performed semiquantitative analyses to measure the mRNA level of Pcdhs in in situ hybridization with the Image J software and the protein level of some Pcdhs by Western blots with antibodies supplied commercially. The results indicated that the

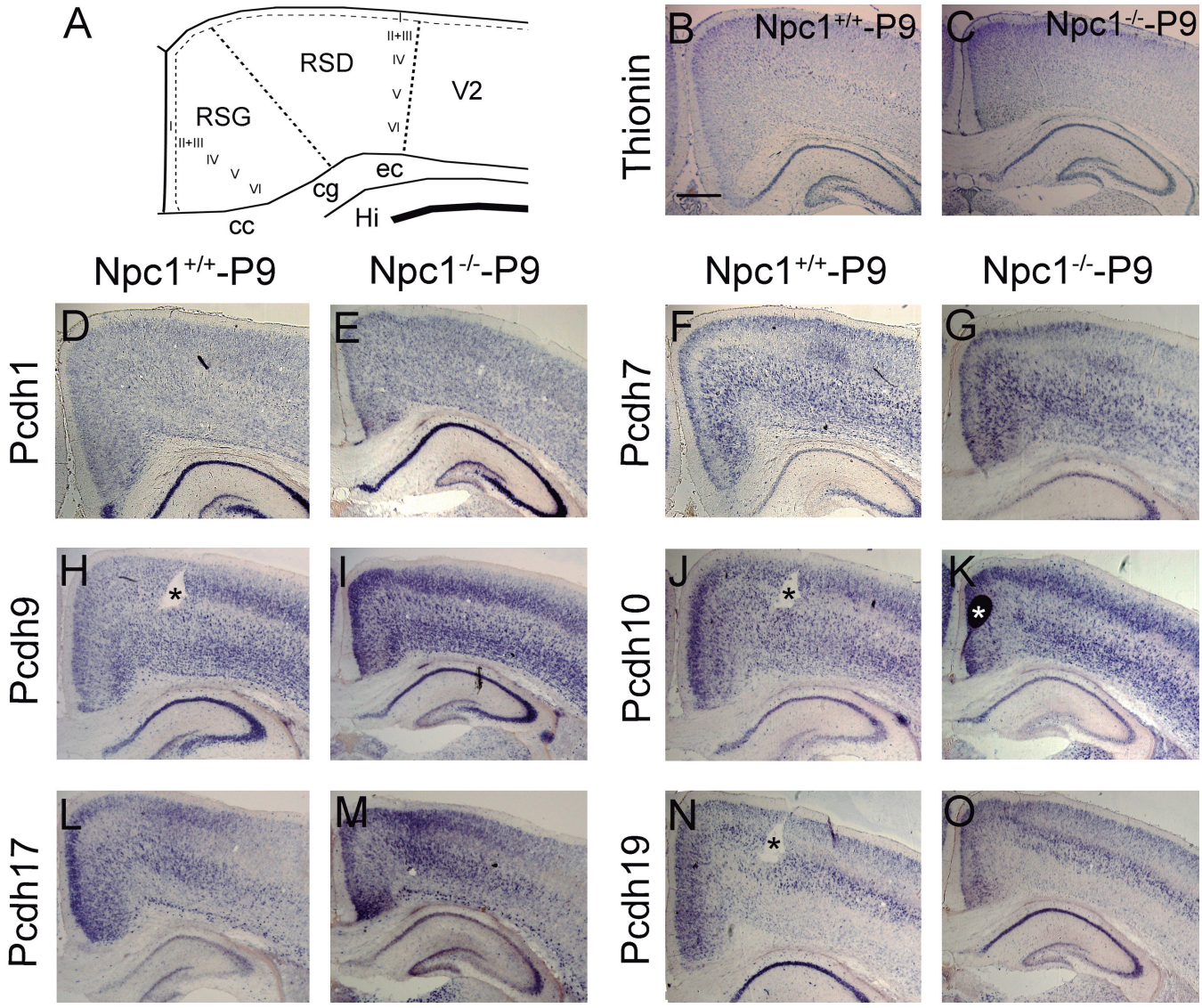

Fig. 1. *In situ* hybridization for Pcdhs in the adjacent transverse sections through retrosplenial dysgranular cortex (RSD), retrosplenial granular cortex (RSG) and visual cortex (V2) at postnatal day (P) 9 in the wild-type (Npc1$^{+/+}$) and NPC1 mutant (Npc1$^{-/-}$) mice. **A.** A schematic overview of the anatomical structures investigated here, I-VI indicates different cortical layers. **B, C.** Thionin staining in similar sections for Npc1$^{+/+}$ and Npc1$^{-/-}$ to identify the different anatomical parts and the cortical layers. **D-O.** *In situ* hybridization of Pcdh1 **(D, E)**, Pcdh7 **(F, G),** Pcdh9 **(H, I)**, Pcdh10 **(J, K)**, Pcdh17 **(L, M)** and Pcdh19 **(N, O**) in the adjacent transverse sections through RSG, RSD and V2 cortex. Asterisks in H, J, K, and N indicate the artificial break or folder. cc, corpus callosum; cg, cingulum; ec, external capsule; Hi, hippocampus; Pcdh, protocadherin; RSD, retrosplenial dysgranular cortex; RSG, retrosplenial granular cortex; Th, thionin. Scale bar: 300 μm in B for all.

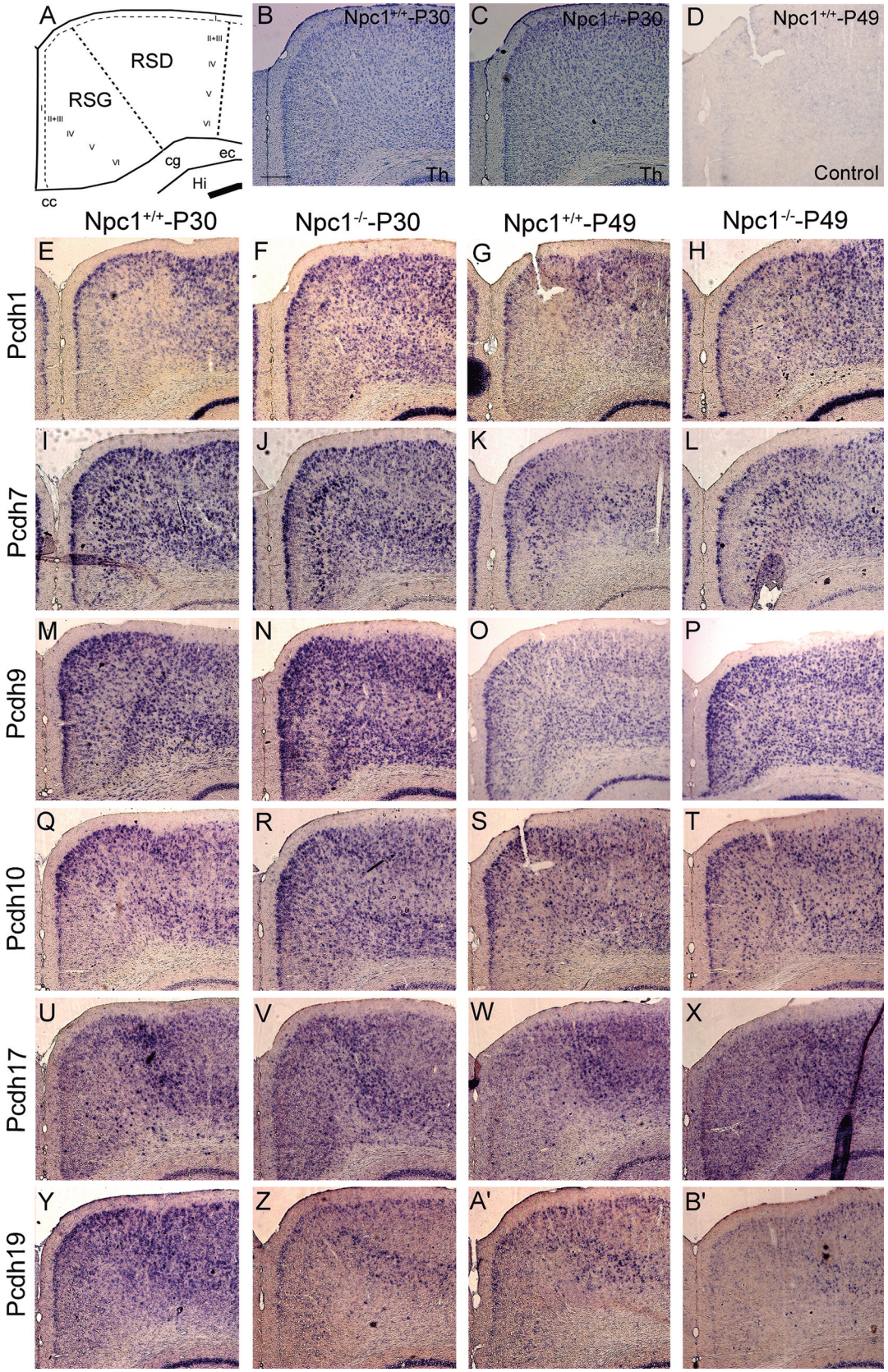

Fig. 2. *In situ* hybridization for Pcdhs in the adjacent transverse sections through retrosplenial dysgranular cortex (RSD) and retrosplenial granular cortex (RSG) at postnatal day (P) 30 and P49 in the wild-type (Npc1+/+) and NPC1 mutant (Npc1$^{-/-}$) mice. **A.** A schematic overview of the anatomical structures investigated here, I-VI indicates different cortical layers. **B, C.** Thionin staining in similar sections for Npc1+/+ and Npc1$^{-/-}$ to identify the different anatomical parts and the cortical layers. **D.** *In situ* hybridization using sense cRNA-probe for Pcdh1 as negative control. **E-B'.** *In situ* hybridization of Pcdh1 **(E-H)**, Pcdh7 **(I-L)**, Pcdh9 **(M-P)**, Pcdh10 **(Q-T)**, Pcdh17 **(U-X)** and Pcdh19 **(Y-B')** in the adjacent transverse sections through RSG and RSD cortex at P30 and P49. cc, corpus callosum; cg, cingulum; ec, external capsule; Hi, hippocampus; Pcdh, protocadherin; RSD, retrosplenial dysgranular cortex; RSG, retrosplenial granular cortex; Th, thionin. Scale bar: 200 μm in B for all.

mRNA amount of Pcdhs in the regions of RSG, RSD and V2 between Npc1$^{-/-}$ and wild type mice was not significantly different (Figs. 4A,B). However, the amounts of Pcdh10 (Fig. 4G,I) and Pcdh17 (Fig. 4H,J) protein in whole tissue lysate of the cerebral cortex were significantly increased in Npc1$^{-/-}$ mice at P9 when compared to the wild type mice (Fig. 4G-J).

Pcdhs expression in RSG and RSD at P30 and P49

In RSG and RSD regions (Fig. 2A), thionin staining revealed that cell distribution and layer structures were similar in both wild-type and Npc1$^{-/-}$ mice (Fig. 2B,C). In wild-type mice, Pcdh1 signals were mainly restricted to layers II-III of the RSG and RSD regions at P30 (Fig. 2E) and P49 (Fig. 2G). However, in Npc1$^{-/-}$ mice, signals were also found in layers IV-VI at corresponding stages (Fig. 2F,H). For Pcdh7, signals were found in all layers in wild-type mice at P30 and decreased at P49, but they were stronger in layers V-VI in Npc1$^{-/-}$ mice (Fig. 2J,L). The expression of Pcdh9 in Npc1$^{-/-}$ mice was stronger than that in wild-type mice, especially in layers II-VI (Fig. 2M-P). In wild-type mice Pcdh10 signals were strong in the RSD cortex and weak in the RSG cortex at P30 (Fig. 2Q), but in Npc1$^{-/-}$ mice signals were stronger in all layers in both regions at P30 (Fig. 2R). The expression patterns of Pcdh17 in both wild-type and Npc1$^{-/-}$ mice were similar, but signals in the RSG region of Npc1$^{-/-}$ mice were stronger than that of wild-type mice (Fig. 2U-X). Finally, the expression of Pcdh19 in Npc1$^{-/-}$ mice was decreased at both P30 and P49, when compared to that in wild-type mice (Fig. 2Y-B').

Furthermore, semiquantitative analyses of the mRNA level by in situ hybridization were evaluated using the Image J software. The results indicated that in the regions of RSG and RSD, the mRNA amount of Pcdh9 was significantly increased at both P30 and P49 in Npc1$^{-/-}$ mice (Fig. 4C,E), but Pcdh19 significantly decreased (Fig. 4C,E) when compared to wild type mice (Fig. 4C,E). The amounts of other Pcdhs, including Pcdh1, Pcdh7, Pcdh10, and Pcdh17 were not significantly different between Npc1$^{-/-}$ and wild type mice (Fig. 4C,E). Moreover, the amounts of both Pcdh10 (Fig. 4G,I) and Pcdh17 (Fig. 4H,J) protein in whole

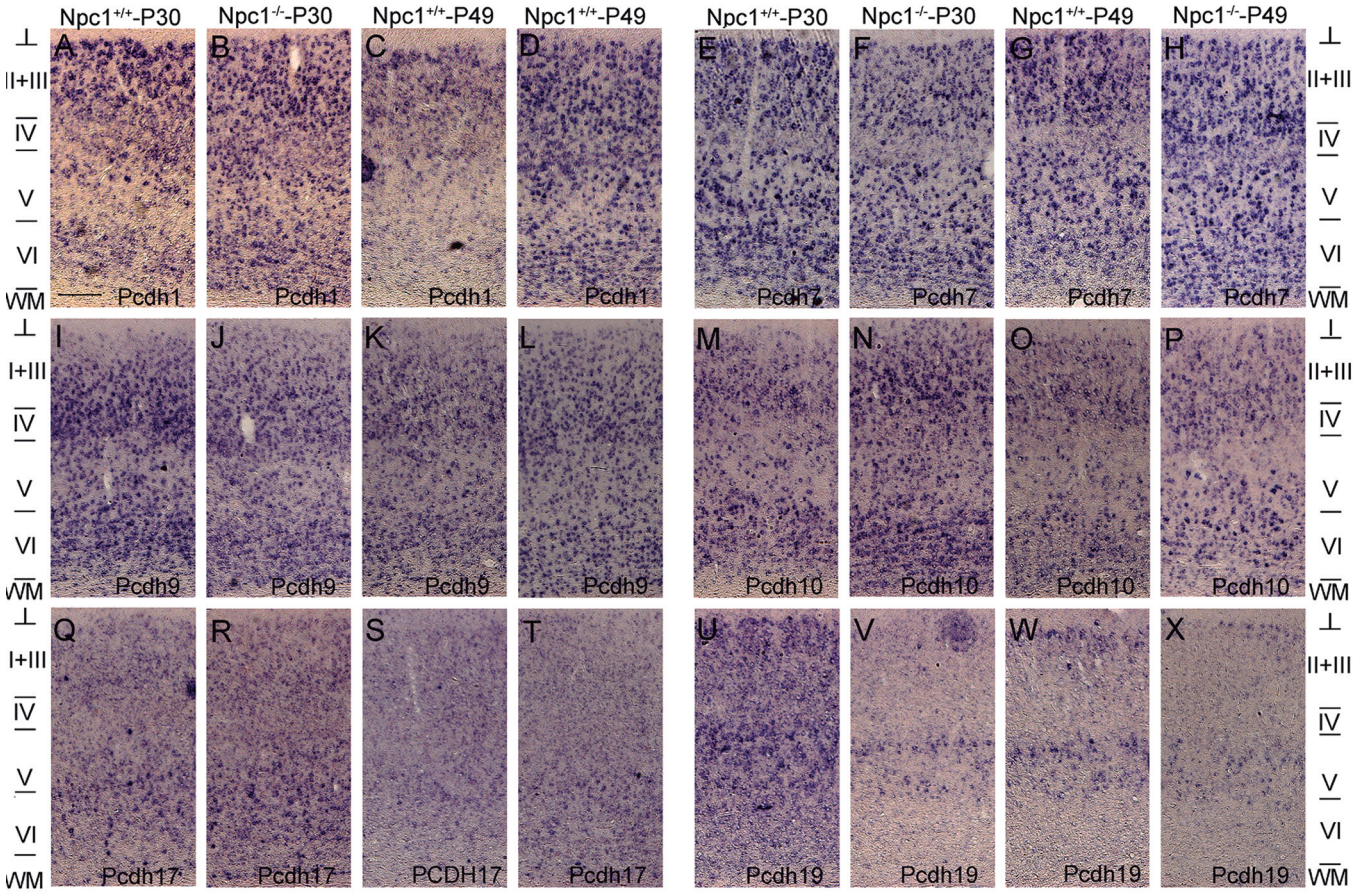

Fig. 3. *In situ* hybridization for Pcdhs in the adjacent transverse sections through the visual cortex V2 in Npc1$^{+/+}$ and Npc1$^{-/-}$ mice with a series of adjacent sections at postnatal day 30 (P30) and 49 (P49), respectively. Results were obtained with cRNA probes for Pcdh1 **(A-D)**, Pcdh7 **(E-H)**, Pcdh9 **(I-L)**, Pcdh10 **(M-P)**, Pcdh17 **(Q-T)** and Pcdh19 **(U-X)**. I-VI indicates different cortical layers; WM, white matter. Scale bar: 200 μm in A for all.

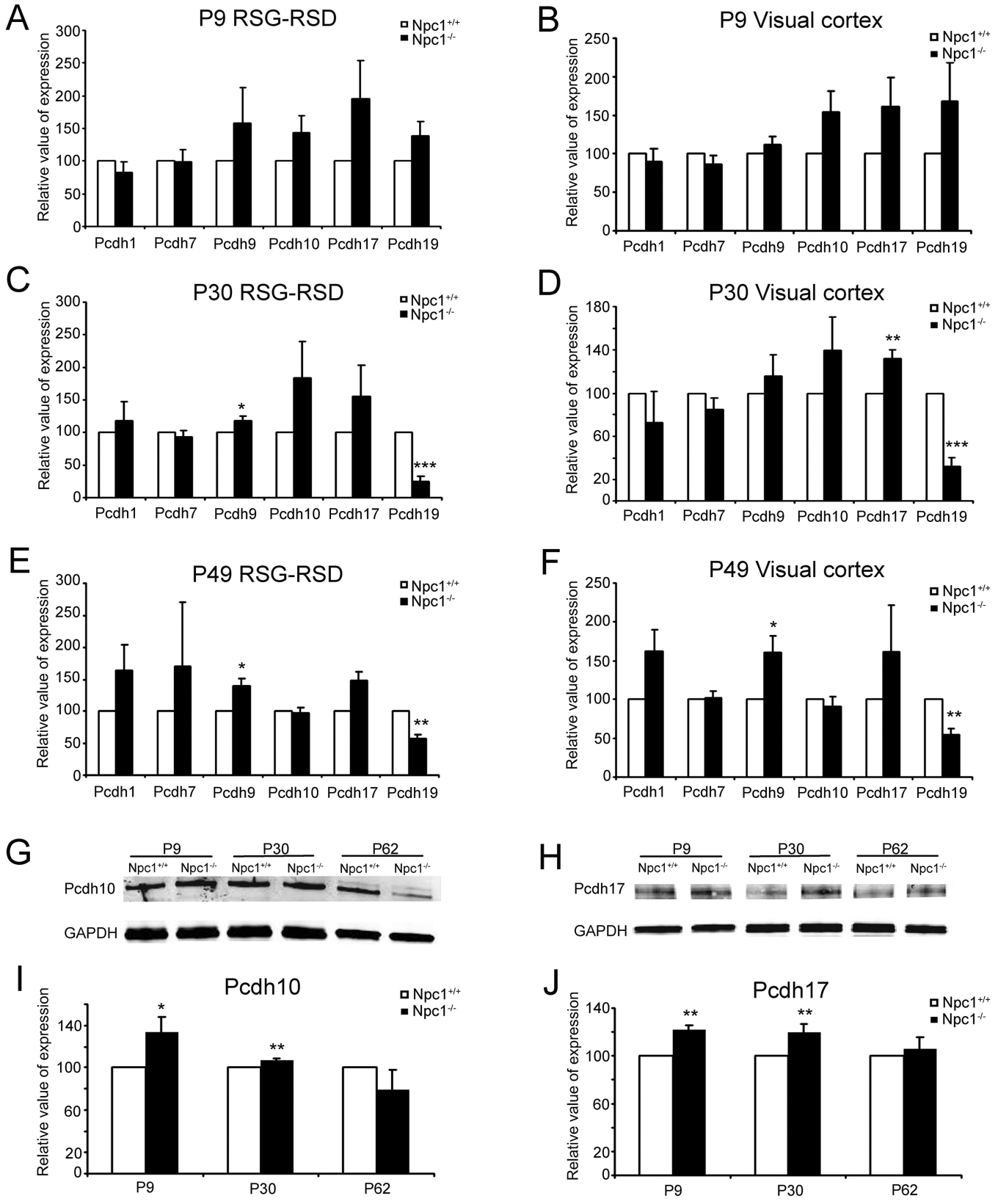

Fig. 4. Quantitative analyses of Pcdhs mRNAs and proteins in the different regions of the Npc1$^{-/-}$ cortex from P9 to P62, compared to the Npc1$^{+/+}$ cortex. **A-F.** Image J software was used to quantify mRNA intensity of Pcdhs in the retrosplenial granular cortex (RSG) and retrosplenial dysgranular cortex (RSD) at P9 **(A)**, P30 **(C)** and P49 **(E)**, in visual cortex V2 at P9 **(B)**, P30 **(D)** and P49 **(F)**. Data are normalized to the control mice and presented as mean ± SEM from at least three independent experiments. * p<0.05, ** p<0.01, *** p<0.001 compared to the control. **G-J.** Western blots and semi-quantitative analyses show the protein levels of Pcdh10 **(G, I)** and Pcdh17 **(H, J)** in the Npc1$^{-/-}$ cortex from P9 to P62 compared to the Npc1+/+ cortex. GAPDH is used as a loading control. Data are normalized by the number of control mice and presented as mean ± SEM from at least three independent experiments. * p<0.05, ** p<0.01 compared to the control.

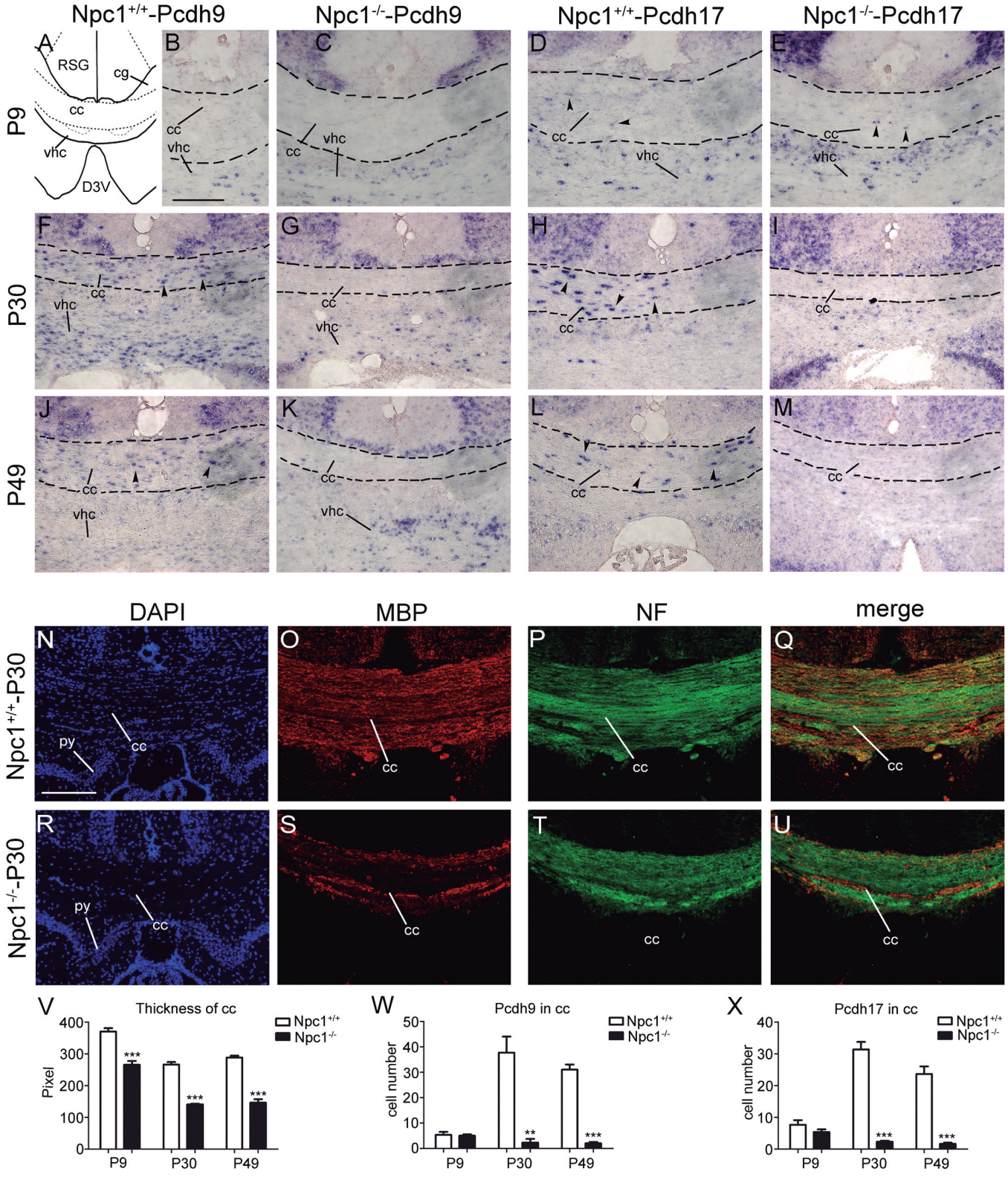

Fig. 5. Decreased expression of Pcdhs in the corpus callusom (cc) of Npc1$^{+/+}$ and Npc1$^{-/-}$ mice. **A.** A schematic overview of the anatomical structures investigated here. **B-M.** Results from in situ hybridization were obtained with cRNA probes for Pcdh9 at postnatal day (P) 9 (**B, C**), P30 (**F, G**), and P49 (**J, K**) and for Pcdh17 at P9 (**D, E**), P30 (**H, I**), and P49 (**L, M**). **N-U.** Co-expression of myelin basic protein (MBP, red) and neurofilament (NF, green) in the cc in Npc1$^{+/+}$ and Npc1$^{-/-}$ mice, detected by double-immunohistochemistry at P30. **V-X.** Comparison of the thickness of corpus callusom (V), Pcdh9-positive cells (W), and Pcdh17-positive cells (X) between Npc1$^{+/+}$ and Npc1$^{-/-}$ mice at different stages. Abbreviations: cc, corpus callosum; vhc, ventral hippocampal commissure; DAPI, cell nuclear staining. Arrows indicate Pcdhs positive cells. ** p<0.01, *** p<0.001 compared to the control. Scale bar: 200 μm in A for all.

tissue lysate of the cerebral cortex were significantly increased in Npc1$^{-/-}$ mice at P30, but not at P62, when compared to the wild type mice (Figs. 4G-J).

Pcdhs expression in the visual cortex V2 at P30 and P49

In wild-type mice, Pcdh1 was mainly restricted to

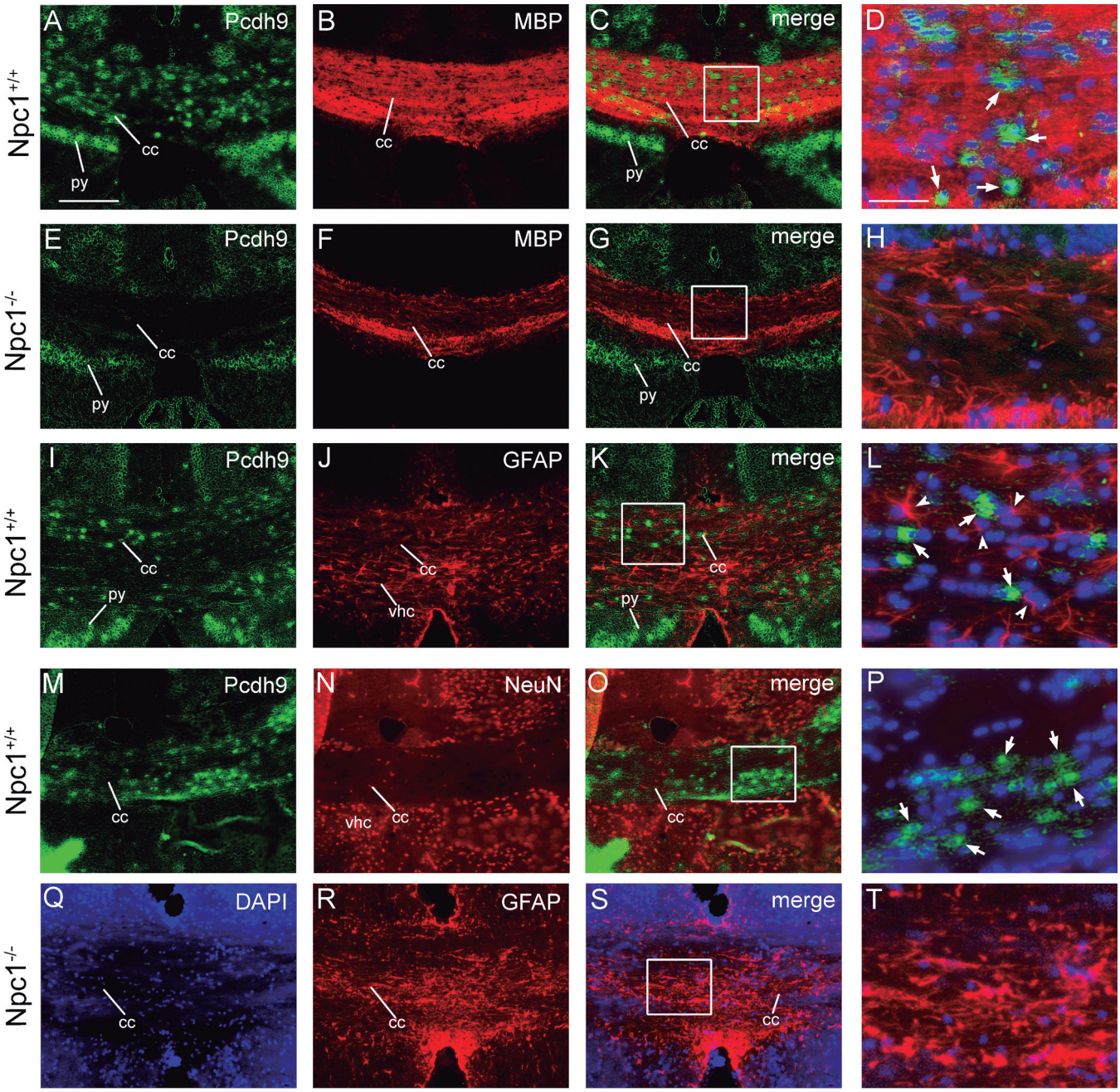

Fig. 6. Pcdh9 expression in the corpus callusom (cc), compared to the expression of different markers for oligodendrocyte - myelin basic protein (MBP), astrocyte - GFAP and neuron - NeuN at P30. **A-D.** Double-labeling in the same section for Pcdh9 (green color) and the oligodendrocyte marker (MBP; red color) in cc of Npc1$^{+/+}$ mice. **E-H.** Double-labeling in the same section for Pcdh9 (green color) and the oligodendrocyte marker (MBP; red color) in the cc of Npc1$^{-/-}$ mice. **I-L.** Double-labeling in the same section for the Pcdh9 (green color) and the astrocyte marker (GFAP; red color) in the cc of Npc1$^{+/+}$ mice. **M-P.** Double-labeling in the same section for the Pcdh9 (green color) and the neuronal marker (NeuN; red color) in the cc of Npc1$^{+/+}$ mice. **Q-T.** Immunolabeling for the astrocyte marker (GFAP; red color) in the cc of Npc1$^{-/-}$ mice. **D, H, L, P, T** show the high magnification of the regions boxed in **C, G, K, O**, and **S**, respectively. Arrows in **D, L, P** indicate the Pcdh9-positive cells. Arrowheads in L indicate astrocytes. Py, pyramidal cell layer of the hippocampus; vhc, ventral hippocampal commissure. Scale bar: 50 um in D for H, L, P; 200 μm in A for the others.

layers II to IV at P30 and P49 (Fig. 3A,C), but in Npc1$^{-/-}$ mice, strong expression was found in all layers at P30 and P49 (Fig. 3B,D). Expression patterns of Pcdh7, Pcdh9, Pcdh10 and Pcdh17 were found to be similar between Npc1$^{-/-}$ mice and wild type mice (Fig. 3E-T). However, Pcdh19 signals were strongly decreased in Npc1$^{-/-}$ mice, although the distribution patterns of Pcdh-positive cells were similar in both cases (Fig 3U-X).

Furthermore, the mRNA level by in situ hybridization was evaluated by semiquantitative analysis. The results indicated that in the region of the visual cortex V2, Pcdh17 and Pcdh9 mRNA amount was significantly increased at P30 (Fig. 4D) and at P49 (Fig. 4F), respectively, but Pcdh19 decreased at both P30 and P49 (Fig. 4D,F) in Npc1$^{-/-}$ mice. The amounts of other Pcdhs, including Pcdh1, Pcdh7, and Pcdh10 were not significantly different between Npc1$^{-/-}$ and wild type mice (Fig. 4D,F).

Pcdhs expression by oligodendrocytes in the corpus callosum

During development, specific neurons in the cortical layer extend their projecting fibers across the corpus callosum (CC) to the contra-lateral hemisphere (Molyneaux et al., 2007). Homophilic adhesion of cadherins, including protocadherins, guides axon pathfinding to the correct terminal position (Treubert-Zimmermann et al., 2002; Leung et al., 2013). Therefore, we further investigated the expression of the

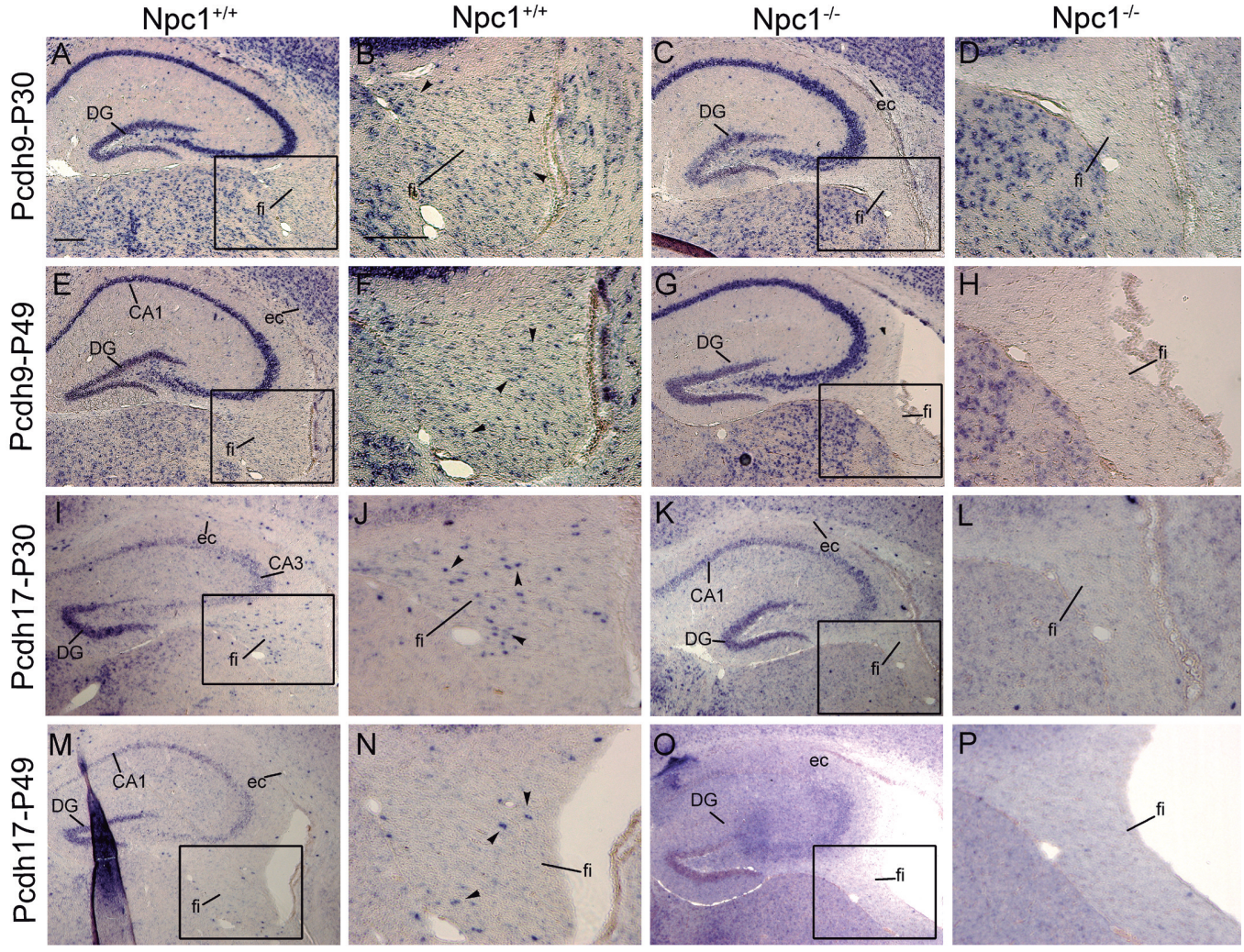

Fig. 7. Expression mapping of Pcdhs in the hippocampus of Npc1$^{+/+}$ and Npc1$^{-/-}$ mice in a series of adjacent sections at postnatal day 30 (P30) and 49 (P49), respectively. Results were obtained with cRNA probes for Pcdh9 **(A-H)** and Pcdh17 **(I-P)**. **B, D, F, H, J, L, N, P** show the high magnification in the regions boxed in **A, C, E, G, I, K, M, O, Q,** respectively. CA1, field CA1 of the hippocampus; CA3, field CA3 of the hippocampus; DG, dentate gyrus; ec, external capsule; fi, fimbria of the hippocampus; LDVL, laterodorsal thalamic nucleus, ventrolateral part. Arrowheads indicate the Pcdhs positive cells. Scale bar: 200 μm in A for C, E, G, I, K, M, O; in B for D, F, H, J, L, N, P.

Pcdhs in the corpus callosum. Generally, our results demonstrated that the number of Pcdh9- and Pcdh17-positive cells and the thickness of the corpus callosum in Npc1$^{-/-}$ mice (Fig. 5B-X), especially at later stages, was decreased, showing a morphological defect (Fig. 5B-U). At P9, only a few Pcdh9- and Pcdh17-positive cells were found in the corpus callosum of both wild-type and Npc1$^{-/-}$ mice (Fig. 5B-E). However, at P30 and P49, the number of Pcdh9- (Fig. 5G,K) and Pcdh17-positive cells (Fig. 5I,M) was significantly decreased in Npc1$^{-/-}$ mice when compared to wild-type mice (Fig. 5F,J,H,L). In adjacent sections, double immunostaining against myelin basic protein (MBP) and neurofilament (NF) showed that MBP was strongly decreased in Npc1$^{-/-}$ mice (Fig. 5S-U) at P30, suggesting a possible defect of oligodendrocytes in the corpus callosum. When quantifying the Pcdh-positive cells in the corpus callosum at P30 and P49, we found that the number of Pcdh9- and Pcdh17-positive cells at P30 and P49 was strongly decreased in Npc1$^{-/-}$ mice compared to the wild type mice (Fig. 5W,X). Furthermore, the thickness of the corpus callosum was significantly decreased in Npc1$^{-/-}$ mice from P9 onwards (Fig. 5V).

To confirm which cell type of the Pcdh-positive cells in the corpus callosum belongs to, we performed double imaging with in situ hybridization for Pcdhs and immunostaining for MBP in the corpus callosum of wild-type mice. The results showed that, e.g., at P30, Pcdh9 mRNA (green in Fig. 6A-P) and the oligodendrocyte marker MBP (red in Fig. 6B-D) were expressed in the same cells (Fig. 6C,D) in the corpus callosum of wild-type mice, but not in Npc1$^{-/-}$ mice (Fig.

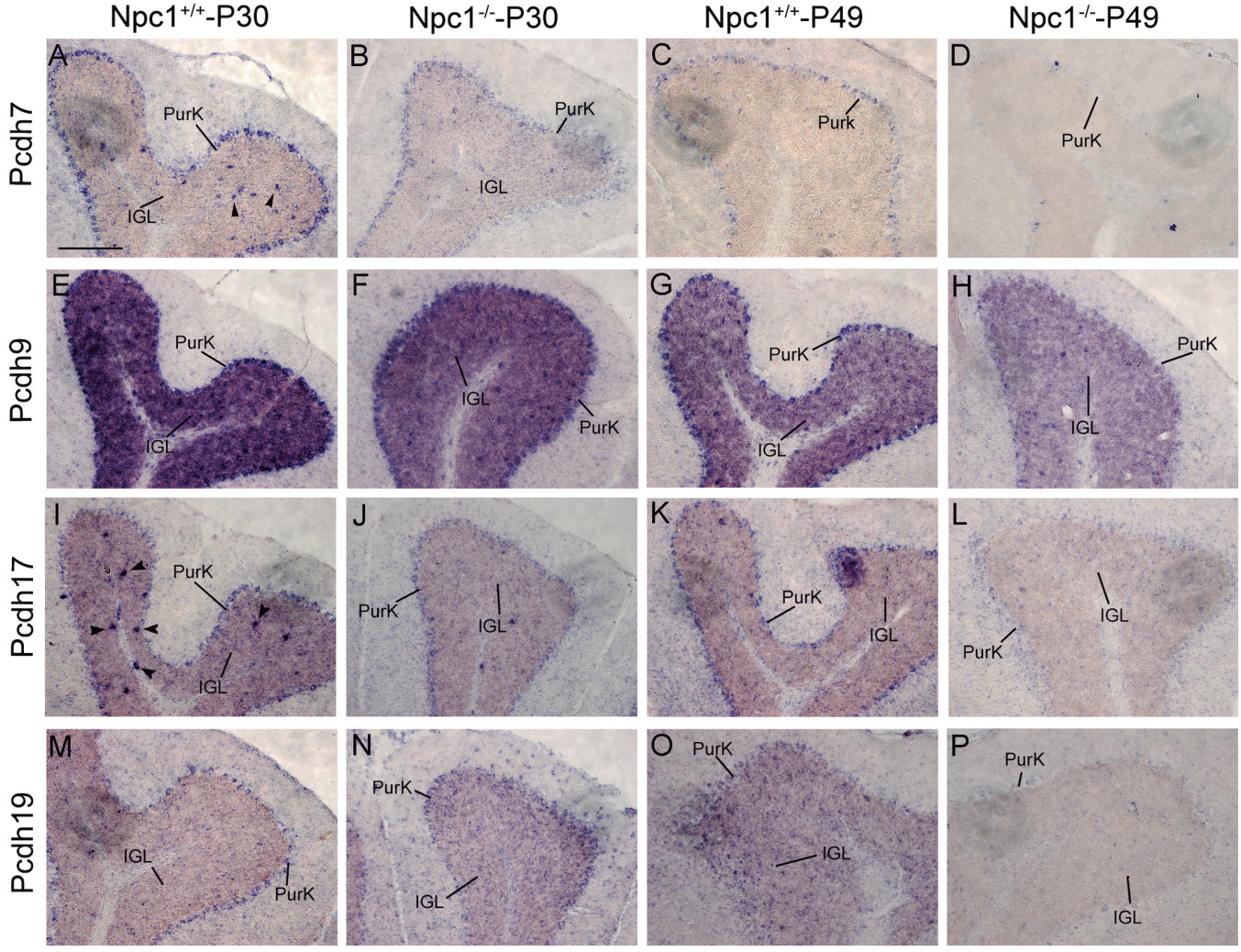

Fig. 8. Expression mapping of Pcdhs in the cerebellum of Npc1$^{+/+}$ and Npc1$^{-/-}$ mice in a series of adjacent sections at postnatal day 30 (P30) and 49 (P49), respectively. Results were obtained with cRNA probes for Pcdh7 **(A-D)**, Pcdh9 **(E-H)**, Pcdh17 **(I-L)** and Pcdh19 **(M-P)**. Arrowheads indicate the Pcdh17-positive cells in IGL. IGl, internal granular layer; Purk, Purkinje cell layer. Scale bar: 200 um in A for all.

6E-H). In contrast, the astrocyte marker GFAP (red in Fig. 6J-L) and the neuronal marker NeuN (red in Fig. 6N-P) were not co-expressed with Pcdh9 mRNA in wild type mice (Fig. 6K,L,O,P), suggesting that the Pcdh-positive cells in the corpus callosum were oligodendrocytes and that their number was decreased in Npc1$^{-/-}$ mice, although the number of astrocytes was increased in Npc1$^{-/-}$ mice (comparing Fig. 6R-T with Fig. 6J-L).

Pcdhs expression in the hippocampus

Furthermore, we investigated expression patterns of the Pcdhs in the hippocampus. Our results showed that the expression patterns of all Pcdhs were conserved between wild-type and Npc1$^{-/-}$ mice (data not shown). For example, Pcdh9 and Pcdh17 were expressed in the CA1, CA2 and CA3 fields and by pyramidal neurons of the dentate gyrus in both wild-type and Npc1$^{-/-}$ mice (Fig. 7A-H and 7I-P). However, in the hippocampal fimbria, we found some differences between wild-type and Npc1$^{-/-}$ mice at later stages. For example, at P30 (Fig. 7A-D, I-L) and P49 (Fig. 7E-H, M-P), the number of the Pcdh9- (Fig. 7D,H) and Pcdh17-positive cells (Fig. 7L,P) was lower in Npc1$^{-/-}$ mice than in wild-type mice (Fig. 7B,F,J,N).

Pcdhs expression in the cerebellum

In the cerebellum, Pcdh-positive cells were found in Purkinje cells and granular cells of the internal granular layer (IGL) in wild-type mice. For example, Pcdh7- (Fig. 8A,C), Pcdh9- (Fig. 8E,G), Pcdh17- (Fig. 8I,K) and Pcdh19-positive cells (Fig. 8M,O) were observed in both the Purkinje cells and granular cells in wild-type mice at P30 and P49, as demonstrated by cell location and morphology, respectively. At P9, we did not find differences of Pcdhs expression by Purkinje cells and granular cells between wild-type and Npc1$^{-/-}$ mice (data not shown). However, the number of the Pcdh7- (Fig. 8B,D), Pcdh9- (Fig. 8F,H), Pcdh17- (Fig. 8J,L), and Pcdh19-positive cells (Fig. 8N,P) of the Purkinje cells and granular cells in Npc1$^{-/-}$ mice was strongly decreased at P30 and P49, respectively. Our data suggest that Pcdhs can be used as markers to monitor the number change of Purkinje cells and granular cells in Npc1$^{-/-}$ mice.

Cadherin mRNA in Npc1 mutant mouse detected by microarray

We did mRNA microarray and obtained transcription profiles across three brain tissues (including forebrain, cerebellum, and hindbrain) for a number of cadherins and protocadherins at P35. Results showed that the mRNA amount of most cadherins and protocadherins exhibited only minor, if any, differences between Npc1$^{-/-}$ and control wild-type mice (e.g., see Fig. 9 for a scatterplot of the forebrain data). An exception is cadherin19 (Cdh19), which is consistently down-regulated in Npc1$^{-/-}$ mice across all tissues, most prominently in the forebrain with a highly significant mean fold change (Fig. 9 and data not shown). Taken together, our data suggest that the distribution of

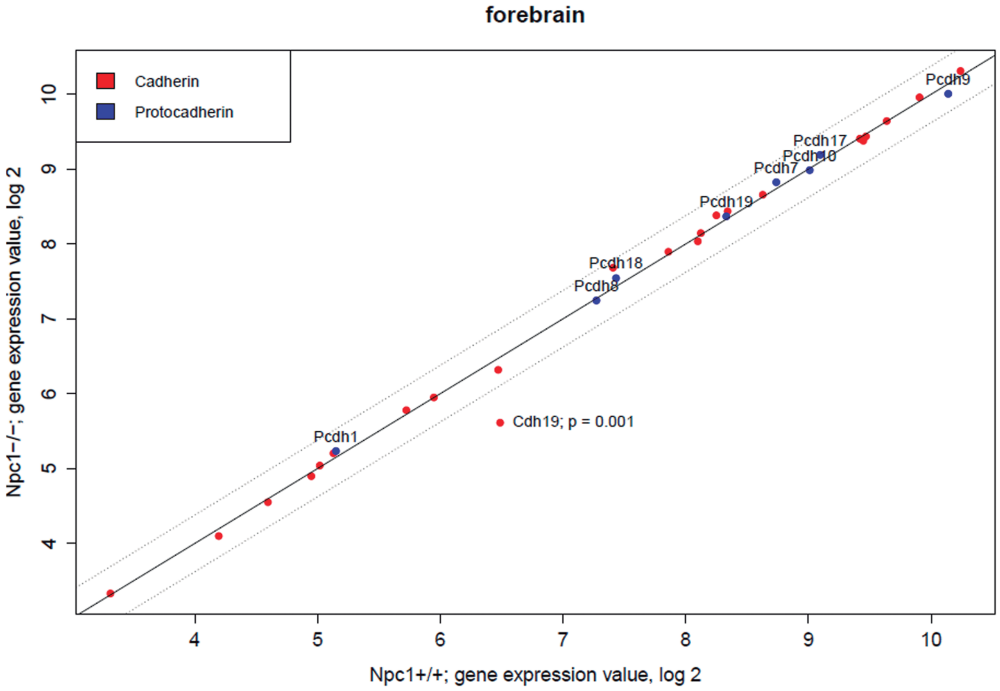

Fig. 9. Scatter-plot of selected mRNA-microarray data from the forebrain tissue at postnatal day 35. Depicted are mean log-transformed signal intensities for cadherin (red) and protocadherin (blue) genes in wild-type mice (controls, X-axis) vs. Npc1$^{-/-}$ mice (Y-axis). Cadherin19 is the only one with the most pronounced differential expression between wild-type and Npc1$^{-/-}$ mice as determined by microarray analysis with a p-value of 0.001 by a two-sided, unpaired t-test at P35. The dotted lines signify a fold change of 1.3 and -1.3 between the groups, respectively.

protocadherins in Npc1$^{-/-}$ mice was altered when compared to wild-type mice, although the mRNA amount of protocadherins in the CNS seems stable at least until P35.

Discussion

The NPC1 disease is characterized by a widespread neurodegeneration, an increased number of astrocytes, and dysmyelination in the cerebral cortex (Ong et al., 2001; Takikita et al., 2004). The Npc1$^{-/-}$ mouse mimics features of the human NPC1 neuropathology (Boothe et al., 1984), including cerebral atrophy, dysmyelination and neuronal degeneration, and cognitive impairment for learning and remembering (German et al., 2002; Võikar et al., 2002; Baudry et al., 2003; Sarna et al., 2003; Hovakimyan et al., 2013). Therefore, it is a useful mouse model to study potential phathomechanisms and therapeutic interactions for the NPC1 disease.

In this study, we showed that in the regions of RSG, RSD, and V2 of the Npc1$^{-/-}$ mouse, although the distribution of some Pcdhs in the cortical layers is altered to be stronger or weaker, the laminar patterns (structures) of Pcdhs still remain (Figs. 1-4), suggesting that Pcdh-mediate adhesion and sorting of early neurons in the cortical development is not abolished by Npc1 mutation.

The corpus callosum is the largest fiber tract in the brain and connects neurons between both cerebral hemispheres. The formation of the corpus callosum is strictly controlled by a large number of molecules, which are involved in, e.g., the formation of glial populations and the guidance of callosal axons (Richards et al., 2004). We showed that the thickness of the corpus callosum in the Npc1$^{-/-}$ mouse is different compared to the wild-type control (Fig. 5), suggesting a defect of the corpus callosum in the Npc1$^{-/-}$ mouse. Interestingly, our data further revealed that Pcdh-positive oligodendrocytes and myelination in the corpus callosum are strongly decreased, accompanied by an increase of GFAP-positive astrocytes. This finding is consistent with the data described previously (Takikita et al., 2004; Pressey et al., 2012). However, the up-regulation of GFAP is not connected with the decreased expression of Pcdhs investigated here, because we found that only oligodendrocytes, but not astrocytes or neurons, express Pcdh9 (Fig. 6). Therefore, the decreased expression of Pcdhs coincides with the loss of oligodendrocytes in the corpus callosum of Npc1$^{-/-}$ mice, suggesting that the Pcdhs, e.g., Pcdh9 and Pcdh17, can be applied as a marker to monitor oligodendrocyte number of the corpus callosum in the Npc1$^{-/-}$ mice.

In the present study, seven Pcdhs were found to be expressed by pyramidal neurons in the CA fields and dentate gyrus of the hippocampus. There was no obvious difference between wild-type and Npc1$^{-/-}$ mice (Fig. 7, data not shown). However, in the hippocampal fimbria region, the expression of Pcdh9 and Pcdh17 was reduced in the Npc1$^{-/-}$ mouse compared to the wild-type mouse (Fig. 7). The precise mechanism of this phenomenon has to be studied further.

Purkinje cell degeneration is a prominent feature of neuropathology in the NPC1 disease. During the early postnatal stage, Purkinje cells exhibit a morphological abnormality with an axonal swelling and cytological accumulation (Sarna et al., 2003), followed by a progressive loss of Purkinje cells in the Npc1$^{-/-}$ mouse at later stages (Sarna et al., 2003; Zhang et al., 2008). Here, our data show that decreased expression of the Pcdhs is compatible with the degeneration of Purkinje cells in the Npc1$^{-/-}$ mouse. It is of interest to know whether the decreased Pcdhs is involved in Purkinje cell degeneration or whether the Pcdhs are only a marker for Purkinje cells, which are degenerated in the Npc1$^{-/-}$ mouse, resulting in the decrease of Pcdhs.

It should be noted that although expressions of Pcdhs in the local regions are either decreased or increased in the Npc1$^{-/-}$ mouse when compared to the wild-type mouse, the mRNA amounts of distinct Pcdhs in the forebrain, the hindbrain and the cerebellum detected by mRNA microarray have only minor changes between them at least at P35 (see Fig. 9). Based on the present data, it is difficult to determine whether the alteration of Pcdhs in the Npc1$^{-/-}$ mouse is caused directly by Npc1 mutation or resulted from the accumulation of lipids in cells. The relationship between them should be further investigated.

Acknowledgements. We thank Dr. Christoph Redies, Dr. Masatoshi Takeichi, Dr. Frans van Roy, and Dr. Shinji Hirano for kind gifts of the plasmids used for in situ hybridization. This work is supported by an FORUN program from University Rostock Medical Center (889012).

References

Ahmed Z.M., Riazuddin S., Ahmad J., Bernstein S.L., Guo Y., Sabar M.F., Sieving P., Riazuddin S., Griffith A.J., Friedman T.B., Belyantseva I.A. and Wilcox E.R. (2003). PCDH15 is expressed in the neurosensory epithelium of the eye and ear and mutant alleles are responsible for both USH1F and DFNB23. Hum. Mol. Genet. 12, 3215-3223.

Alagramam K.N., Murcia C.L., Kwon H.Y., Pawlowski K.S., Wright C.G. and Woychik R.P. (2001). The mouse Ames waltzer hearing-loss mutant is caused by mutation of Pcdh15, a novel protocadherin gene. Nat. Genet. 27, 99-102.

Aoki E., Kimura R., Suzuki S.T. and Hirano S. (2003). Distribution of OL-protocadherin protein in correlation with specific neural compartments and local circuits in the postnatal mouse brain. Neuroscience 117, 593-614.

Bauer P., Knoblich R., Bauer C., Finckh U., Hufen A., Kropp J., Braun S., Kustermann-Kuhn B., Schmidt D., Harzer K. and Rolfs A. (2002). NPC1: Complete genomic sequence, mutation analysis, and characterization of haplotypes. Hum. Mutat. 19, 30-38.

Baudry M., Yao Y., Simmons D., Liu J. and Bi X. (2003). Postnatal development of inflammation in a murine model of Niemann-Pick type C disease: immunohistochemical observations of microglia and astroglia. Exp. Neurol. 184, 887-903.

Bolstad B.M., Collin F., Simpson K.M., Irizarry R.A. and Speed T.P. (2004). Experimental design and low-level analysis of microarray data. Int. Rev. Neurobiol. 60, 25-58.

Bolstad B.M., Collin F., Brettschneider J., Simpson K., Cope L., Irizarry R.A. and Speed T.P. (2005). Quality assessment of affymetrix GeneChip data. In: Bioinformatics and Computational Biology Solutions Using R and Bioconductor. Gentleman R., Carey V., Huber W., Irizarry R. and Dudoit S. (eds.) Springer. NY. pp 33-47.

Boothe A.D., Weintroub H., Pentchev P.G., Jones J., Butler J., Barry J.E., Neumeyer B., Stivers J.A. and Brady R.O. (1984). A lysosomal storage disorder in the BALB/c mouse: bone marrow transplantation. Vet. Pathol. 21, 432-441.

Brettschneider J., Collin F., Bolstad B.M. and Speed T.P. (2008). Quality assessment for short oligonucleotide microarray data. Technometrics 50, 241-264.

Carstea E.D., Morris J.A., Coleman K.G., Loftus S.K., Zhang D., Cummings C., Gu J., Rosenfeld M.A., Pavan W.J., Krizman D.B., Nagle J., Polymeropoulos M.H., Sturley S.L., Ioannou Y.A., Higgins M.E., Comly M., Cooney A., Brown A., Kaneski C.R., Blanchette-Mackie E.J., Dwyer N.K., Neufeld E.B., Chang T.Y., Liscum L., Strauss J.F., Ohno K., Zeigler M., Carmi R., Sokol J., Markie D., O'Neill R.R., van Diggelen O.P., Elleder M., Patterson M.C., Brady R.O., Vanier M.T., Pentchev P.G. and Tagle D.A. (1997). Niemann-Pick C1 disease gene: homology to mediators of cholesterol homeostasis. Science 277, 228-231.

Emond M.R., Biswas S. and Jontes J.D. (2009). Protocadherin-19 is essential for early steps in brain morphogenesis. Dev. Biol. 334, 72-83.

Franklin Keith B.J. and Paxinos G. (2007). The mouse brain in stereotaxic coordinates (Third Edition). Academic Press. New York.

German D.C., Liang C.L., Song T., Yazdani U., Xie C. and Dietschy J.M. (2002). Neurodegeneration in the Niemann-Pick C mouse: glial involvement. Neuroscience 109, 437-450.

Hertel N. and Redies C. (2011). Absence of layer-specific cadherin expression profiles in the neocortex of the reeler mutant mouse. Cereb. Cortex 21, 1105-1117.

Hirano S. (2007). Pioneers in the ventral telencephalon: The role of OL-protocadherin-dependent striatal axon growth in neuralcircuit formation. Cell Adh. Migr. 1, 76-78.

Hirano S., Suzuki S.T. and Redies C. (2003). The cadherin superfamily in neural development: diversity, function and interaction with other molecules. Front. Biosci. 8, d306-d355.

Homayouni R., Rice D.S. and Curran T. (2001). Disabled-1 interacts with a novel developmentally regulated protocadherin. Biochem. Biophys. Res. Commun. 289, 539-547.

Hovakimyan M., Maass F., Petersen J., Holzmann C., Witt M., Lukas J., Frech M.J., Hübner R., Rolfs A. and Wree A. (2013). Combined therapy with cyclodextrin/allopregnanolone and miglustat improves motor but not cognitive functions in Niemann-Pick Type C1 mice. Neuroscience 252, 201-211.

Hulpiau P. and van Roy F. (2009). Molecular evolution of the cadherin superfamily. Int. J. Biochem. Cell Biol. 41, 349-369.

Irizarry R.A., Hobbs B., Collin F., Beazer-Barclay Y.D., Antonellis K.J., Scherf U. and Speed T.P. (2003). Exploration, normalization, and summaries of high density oligonucleotide array probe level data. Biostatistics 4, 249-264.

Jamal S.M., Basran R.K., Newton S., Wang Z. and Milunsky J.M. (2010). Novel de novo PCDH19 mutations in three unrelated females with epilepsy female restricted mental retardation syndrome. Am. J. Med. Genet. A 152A, 2475-2481.

Kahr I., Vandepoele K. and van Roy F. (2013). Delta-protocadherins in health and disease. Prog. Mol. Biol. Transl. Sci. 116, 169-192.

Krishna-K K., Hertel N. and Redies C. (2011). Cadherin expression in the somatosensory cortex: evidence for a combinatorial molecular code at the single-cell level. Neuroscience 175, 37-48.

Leung LC., Urbancic V., Baudet M.L., Dwivedy A., Bayley T.G., Lee A.C., Harris W.A. and Holt C.E. (2013). Coupling of NF-protocadherin signaling to axon guidance by cue-induced translation. Nat. Neurosci. 16, 166-173.

Lin J., Luo J. and Redies C. (2010). Cadherin-19 expression is restricted to myelin-forming cells in the chicken embryo. Neuroscience 165, 168-178.

Lin J., Yan X., Wang C., Talabattula V.A., Guo Z., Rolfs A. and Luo J. (2013). Expression patterns of the ADAMs in early developing chicken cochlea. Dev. Growth. Differ. 55, 368-376.

Liu Q., Chen Y., Pan J.J. and Murakami T. (2009). Expression of protocadherin-9 and protocadherin-17 in the nervous system of the embryonic zebrafish. Gene Expr. Patterns 9, 490-496.

Liu Q., Chen Y., Kubota F., Pan J.J. and Murakami T. (2010). Expression of protocadherin-19 in the nervous system of the embryonic zebrafish. Int. J. Dev. Biol. 54, 905-911.

Loftus S.K., Morris J.A., Carstea E.D., Gu J.Z., Cummings C., Brown A., Ellison J., Ohno K., Rosenfeld M.A., Tagle D.A., Pentchev P.G. and Pavan W.J. (1997). Murine model of Niemann-Pick C disease: mutation in a cholesterol homeostasis gene. Science 277, 232-235.

Luan Z., Saito Y., Miyata H., Ohama E., Ninomiya H. and Ohno K. (2008). Brainstem neuropathology in a mouse model of Niemann-Pick disease type C. J. Neurol. Sci. 268, 108-116.

Luo J., Treubert-Zimmermann U. and Redies C. (2004). Cadherins guide migrating Purkinje cells to specific parasagittal domains during cerebellar development. Mol. Cell Neurosci. 25, 138-152.

Miar A., Alvarez V., Corao A.I., Alonso B., Díaz M., Menéndez M., Martínez C., Calatayud M., Morís G. and Coto E. (2011). Lack of association between protocadherin 11-X/Y (PCDH11X and PCDH11Y) polymorphisms and late onset Alzheimer's disease. Brain Res. 1383, 252-256.

Miyake K., Hirasawa T., Soutome M., Itoh M., Goto Y., Endoh K., Takahashi K., Kudo S., Nakagawa T., Yokoi S., Taira T., Inazawa J. and Kubota T. (2011). The protocadherins, PCDHB1 and PCDH7, are regulated by MeCP2 in neuronal cells and brain tissues: implication for pathogenesis of Rett syndrome. BMC Neurosci. 12, 81.

Molyneaux B.J., Arlotta P., Menezes J.R. and Macklis J.D. (2007). Neuronal subtype specification in the cerebral cortex. Nat. Rev. Neurosci. 8, 427-437.

Naureckiene S., Sleat D.E., Lackland H., Fensom A., Vanier M.T., Wattiaux R., Jadot M. and Lobel P. (2000). Identification of HE1 as the second gene of Niemann-Pick C disease. Science 290, 2298-2301.

Ong W.Y., Kumar U., Switzer R.C., Sidhu A., Suresh G., Hu C.Y. and Patel S.C. (2001). Neurodegeneration in Niemann-Pick type C disease mice. Exp. Brain Res. 141, 218-231.

Ostergaard E., Batbayli M., Duno M., Vilhelmsen K., and Rosenberg T. (2010). Mutations in PCDH21 cause autosomal recessive cone-rod dystrophy. J. Med. Genet. 47, 665-669.

Pentchev P.G., Boothe A.D., Kruth H.S., Weintroub H., Stivers J. and Brady R.O. (1984). A genetic storage disorder in BALB/C mice with a metabolic block in esterification of exogenous cholesterol. J. Biol.

Chem. 259, 5784-5791.

Pressey S.N., Smith D.A., Wong A.M., Platt F.M. and Cooper J.D. (2012). Early glial activation, synaptic changes and axonal pathology in the thalamocortical system of Niemann-Pick type C1 mice. Neurobiol. Dis. 45, 1086-1100.

Redies C., Treubert-Zimmermann U. and Luo J. (2003). Cadherins as regulators for the emergence of neural nets from embryonic divisions. J. Physiol. Paris 97, 5-15.

Redies C., Vanhalst K. and Roy F. (2005). delta-Protocadherins: unique structures and functions. Cell Mol. Life Sci. 62, 2840-2852.

Redies C., Heyder J., Kohoutek T., Staes K. and Van Roy F. (2008). Expression of protocadherin-1 (Pcdh1) during mouse development. Dev. Dyn. 237, 2496-2505.

Redies C., Neudert F. and Lin J. (2011). Cadherins in cerebellar development: translation of embryonic patterning into mature functional compartmentalization. Cerebellum 10, 393-408.

Redies C., Hertel N. and Hübner C.A. (2012). Cadherins and neuropsychiatric disorders. Brain Res. 1470, 130-144.

Richards L.J., Plachez C. and Ren T. (2004). Mechanisms regulating the development of the corpus callosum and its agenesis in mouse and human. Clin. Genet. 66, 276-289.

Sarna J.R., Larouche M., Marzban H., Sillitoe R.V., Rancourt D.E. and Hawkes R. (2003). Patterned Purkinje cell degeneration in mouse models of Niemann-Pick type C disease. J. Comp. Neurol. 456, 279-291.

Sliwinska-Kowalska M. and Pawelczyk M. (2013). Contribution of genetic factors to noise-induced hearing loss: a human studies review. Mutat. Res. 752, 61-65.

Takeichi M. (2007). The cadherin superfamily in neuronal connections and interactions. Nat. Rev. Neurosci. 8, 11-20.

Takikita S., Fukuda T., Mohri I., Yagi T. and Suzuki K. (2004). Perturbed myelination process of premyelinating oligodendrocyte in Niemann-Pick type C mouse. J. Neuropathol. Exp. Neurol. 63, 660-673.

Treubert-Zimmermann U., Heyers D. and Redies C. (2002) Targeting axons to specific fiber tracts in vivo by altering cadherin expression. J. Neurosci. 22, 7617-7626.

Tsai N.P., Wilkerson J.R., Guo W., Maksimova M.A., DeMartino G.N., Cowan C.W. and Huber K.M. (2012). Multiple autism-linked genes mediate synapse elimination via proteasomal degradation of a synaptic scaffold PSD-95. Cell 151, 1581-1594.

Uemura M., Nakao S., Suzuki S.T., Takeichi M. and Hirano S. (2007). OL-Protocadherin is essential for growth of striatal axons and thalamocortical projections. Nat. Neurosci. 10, 1151-1159.

Vanier M.T. and Millat G. (2003). Niemann-Pick disease type C. Clin. Genet. 64, 269-281.

Võikar V., Rauvala H. and Ikonen E. (2002). Cognitive deficit and development of motor impairment in a mouse model of Niemann-Pick type C disease. Behav. Brain Res. 132, 1-10.

Wang C., Yu G., Liu J., Wang J., Zhang Y., Zhang X., Zhou Z. and Huang Z. (2012). Downregulation of PCDH9 predicts prognosis for patients with glioma. J. Clin. Neurosci. 19, 541-545.

Yagi T. and Takeichi M. (2000). Cadherin superfamily genes: functions, genomic organization, and neurologic diversity. Genes Dev. 14, 1169-1180.

Yan X., Lukas J., Witt M., Wree A., Hübner R., Frech M., Köhling R., Rolfs A. and Luo J. (2011). Decreased expression of myelin gene regulatory factor in Niemann-Pick type C 1 mouse. Metab. Brain Dis. 26, 299-306.

Zhang M., Strnatka D., Donohue C., Hallows J.L., Vincent I. and Erickson R.P. (2008). Astrocyte-only Npc1 reduces neuronal cholesterol and triples life span of $Npc1^{-/-}$ mice. J. Neurosci. Res. 86, 2848-2856.

Accepted March 26, 2014